Putting Enhanced Chemical Reactivity in Water Microdroplets Under the Microscope: The Case of a Diels-Alder Reaction

Ke Gong,[#,1] Abhijit Nandy,[#,2] Zhexuan Song,[1] Quansong Li,[1] Ali Hassanali,[3] Giuseppe Cassone,[*,4] Shibdas Banerjee,[*,2] Jing Xie[*,1]

[1]Key Laboratory of Cluster Science of Ministry of Education, Beijing Key Laboratory of Photoelectronic/Electrophotonic Conversion Materials, School of Chemistry and Chemical Engineering, Beijing Institute of Technology, Beijing 100081, China

[2]Department of Chemistry, Indian Institute of Science Education and Research Tirupati, Tirupati 517507, India

[3]International Centre for Theoretical Physics (ICTP), 34151 Trieste, Italy

[4] Institute for Physical-Chemical Processes, Italian National Research Council (CNR-IPCF), 98158 Messina, Italy

[*]Emails: giuseppe.cassone@ipcf.cnr.it; shibdas@iisertirupati.ac.in; jingxie@bit.edu.cn

ABSTRACT: Often, chemical reactions are markedly accelerated in microdroplets compared to the corresponding bulk-phase. While identifying the precise causative factors remains challenging, the interfacial electric field (IEF) and partial solvation are the two widely proposed factors, accounting for the acceleration or turning on many reactions in microdroplets. In sharp contrast, this combined computational and experimental study demonstrates that these two critical factors have negligible effect on promoting a model Diels-Alder (DA) reaction between cyclopentadiene and acrylonitrile in water microdroplets. Instead, the acceleration of the DA reaction is driven by the effect of confinement. Quantum chemical calculations and *ab initio* molecular dynamics simulations coupled with enhanced sampling techniques predict that the air-water interface exhibits a higher free-energy barrier of this reaction than the bulk, while external electric fields marginally reduce the barrier. Remarkably, the catalytic capability of the IEF at the water microdroplet surface is largely hampered by its fluctuating character. Mass spectrometric assessment of the microdroplet reaction corroborate these findings, showing that the DA reaction is not facilitated by the IEF as increasing the spray potential suppresses the DA products by promoting substrate oxidation. While the DA reaction exhibits a surface preference in water microdroplets, the same reaction tends to occur mainly within the core of the acetonitrile microdroplet, suggesting the partial solvation is not necessarily a critical factor for accelerating this reaction in microdroplets. Moreover, experiments indicate that the rapid evaporation of microdroplets and the subsequent reagent enrichment (confinement) caused the observed acceleration of the DA reaction in water microdroplets.

INTRODUCTION

Converting bulk water into micron-sized droplets renders it to behave unusually, often facilitating the chemical transformation of species dissolved in it. The recent surge in such water microdroplet chemistry has been enriched by various studies, which include observations of accelerated reaction rates,[1-5] the promotion of unusual chemical reactions,[6-26]and the stabilization of highly reactive intermediates at the air-water interface.[27-29] The cause of such multifaceted chemistry, preferably at the air-water interface of microdroplets, is often attributed to a multitude of variables that the reactant species experiences at different extents depending upon the nature of the reactant. Some of the important variables driving the water microdroplet chemistry are identified to be: i) high intrinsic electric fields ($\approx 10^9$ V/m) at the droplet surface,[5, 22, 30-32] ii) orientation of reactant(s) at the droplet surface,[15] iii) partial solvation of reactant(s) at the air-water interface,[33-34] iv) droplet surface polarity or pH (acidity/basicity),[1, 35-39] v) confinement of reactants/reagents in small space,[4, 37, 40] vi) evaporation of droplet and thereby sizes and associated lifetimes.[4, 41-45] Besides, impurities like ozone or other reactive oxygen species at the microdroplet interface has also been proposed to influence the interfacial chemistry in microdroplets.[46-48] This study aims to investigate the possible impact of those factors on a typical Diels-Alder (DA) reaction that may occur at or nearby to the water microdroplet surface.

The DA cycloaddition reaction represents one of the most important organic chemical reactions since its discovery in 1928 and is widely used in the total synthesis of complex products.[49-52] In the pioneering work of Breslow and co-workers,[53-55] they found that DA cycloadditions were accelerated by several hundred-folds in water as compared to the reaction conducted in organic solvents. This seminal discovery suggested that the poor solubility of hydrophobic reagents may promote, rather than hamper, certain classes of reactions. In 2005, Sharples and co-workers reported substantial rate acceleration when insoluble reactants are stirred in aqueous suspension, termed "on water" chemistry, for a series of reactions, including the DA cycloaddition of diethyl azodicarboxylate (DEAD) and quadricyclane, among others.[56] While a past study indicated that the DA reaction is less favoured over other side-reaction(s) in water microdroplets,[57] exceptions are noted in the literature with the use of strained multi-cyclic hydrocarbon[58] or 'quasi-benzyne' intermediate.[59] In addition, the Coote group reported electrostatic catalysis of DA reaction using scanning tunnelling microscopy. [60]

https://doi.org/10.26434/chemrxiv-2024-wwgs1 **ORCID:** https://orcid.org/0000-0001-9676-5734 Content not peer-reviewed by ChemRxiv. **License:** CC BY 4.0

Herein, we combined computations and experiments to investigate the factors influencing a model DA reaction (Scheme 1) between cyclopentadiene (CPD) and acrylonitrile (ALT) in water microdroplets, especially to examine the impact of two factors, interfacial electric fields (IEF) and partial solvation.

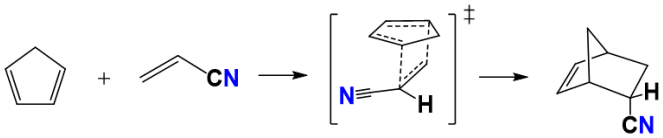

Scheme1. Diels-Alder reaction between cyclopentadiene (CPD) and acrylonitrile (ALT).

Simulations predict that the cumulative effect of partial solvation and IEF cannot promote the DA reaction in water microdroplets. In fact, the barrier of the modeled DA reaction is higher at the air-water interface than in the bulk and this barrier is only slightly lowered under uniform external electric fields. Moreover, the IEF at the surface of water microdroplet is found to fluctuate continuously, a circumstance mitigating the overall electrostatic catalytic capability carried by the field. Microdroplet experiments with water and acetonitrile independently affirm these predictions and find instead that confinement effect is the key factor that increases the rate of the DA reactions in microdroplets. This work elucidates the nuanced role of microdroplet interfaces in chemical reactivity, offering insights into optimizing reaction conditions for potential synthetic applications.

METHODOLOGY

Ab Initio Molecular Dynamics (AIMD) and Metadynamics (MetD) Simulations

To explicitly account for the effects carried by partial solvation on the DA reaction, we performed Born−Oppenheimer AIMD simulations combined with a well-tempered MetD approach using the CP2K package.[61-62] Simulations started from the reactant complex (RC) state, and aimed at determining the free-energy barriers of the reaction in the gas phase, at the air-water interface, and in the bulk. As for the simulation in the gas phase and in the bulk, the cubic box size was 12 Å × 12 Å × 12 Å. The bulk model includes 52 water molecules and one reactant (i.e., CPD+ALT). As far as the AIMD+MetD simulations of the water interface are concerned, water slabs containing up to 200 water molecules were constructed (Figure S1).

Both simulations in the bulk and at the interface were preliminarily equilibrated for at least 5 ps keeping the RC fixed whereas water molecules were allowed to relax. All AIMD+MetD simulations were conducted employing the dispersion-corrected BLYP-D3 exchange and correlation functional with DZVP-MOLOPT-SR-GTH basis set.[63-66] The energy cutoff was set to 400 Ry. The self-consistent field cycle was converged using the orbital transformation method. The dynamics of the system was simulated classically within the NVT ensemble with a timestep of 1 fs. The average temperature was controlled at 300 K using a Nose−Hoover thermostat chain with a coupling time constant of 50 fs. The distances between two pairs of C-C atoms, i.e. C1-C4 and C2-C3 distances, were selected as the collective variables (CVs) for this study (Figure 1). Additionally, block average analysis was performed on the calculated free-energy barriers and on the chosen CVs of the TSs for all the investigated systems to estimate the associated error bars. A more detailed description along with additional results of all the AIMD+MetD simulations can be found in the Supporting Information.

Density Functional Theory (DFT) Calculations. DFT calculations were performed using the Gaussian16 software package.[67] The M06-2X hybrid meta-GGA functional in combination with a 6-311++G(d,p) basis set was used.[68-69] A benchmark preliminary investigation is provided in the Supporting Information (Table S1) to validate the choice of this level of theory. An implicit solvent polarizable continuum model (PCM) was used to model the aqueous phase. Vibrational frequencies were calculated to confirm the nature of all stationary points found and to ascertain that potential energy minima have no imaginary frequencies whilst transition states (TSs) exhibit only one imaginary frequency. Intrinsic reaction coordinate (IRC) calculations were performed on each TS to identify the minimum energy path in this kind of calculation.

The effects produced by static and homogeneous external electric fields (EEFs) were studied using the "Field = M ± N" keyword in Gaussian 16, where M defines the axis of the EEF, ± the direction of the field along the axis, and N its magnitude. EEF strengths in the range [−0.1; +0.1] V/Å were explored. EEFs were applied along the direction of formation of the C-C bond, which we aligned along the Z-axis of our reference system, and along orthogonal directions, namely X, and Y (Figure 1).

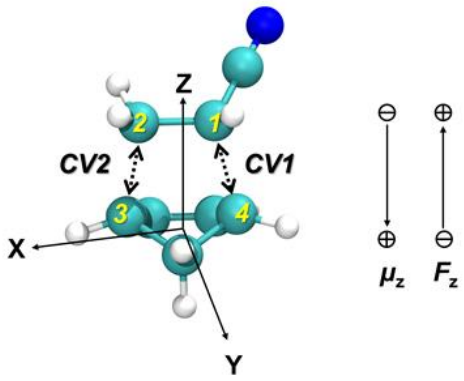

Figure 1. Representations of the reference system adopted for describing the DA reaction between cyclopentadiene (bottom) and acrylonitrile (top) along with the chosen collective variables (CV1 and CV2). Right panel defines the direction of the dipole moment (μ_z) and the external electric field (F_z) along z-axis.

RESULTS AND DISCUSSION

Effects of partial solvation. The free-energy landscapes of the DA reaction between cyclopentadiene (CPD) and acrylonitrile (ALT) to form endo-type product were computed for the reaction in the bulk (Figure 2a), at air-water interface (Figure 2b), and in gas phase (Figure S2) by performing AIMD+MetD simulations. The reaction proceeds through a pre-reaction complex (RC) and a transition state (TS) before forming the product (P) (Figure 2c). The computed internal free-energy barrier $\Delta G^{\ddagger}_{int}$, which equals G(TS) – G(RC), increases from 18.2 kcal/mol in the bulk to 19.2 kcal/mol at the air-water interface, and to 20.7 kcal/mol in the gas phase. This trend of an increasing barrier from bulk to the gas phase agrees rather well with our DFT calculations performed at a higher theory level (Figure S13). The

https://doi.org/10.26434/chemrxiv-2024-wwgs1 **ORCID:** https://orcid.org/0000-0001-9676-5734 Content not peer-reviewed by ChemRxiv. **License:** CC BY 4.0

observation that the free-energy barrier associated with the reaction occurring at the interface being slightly higher than its bulk counterpart is consistent to previous works.[70-71]

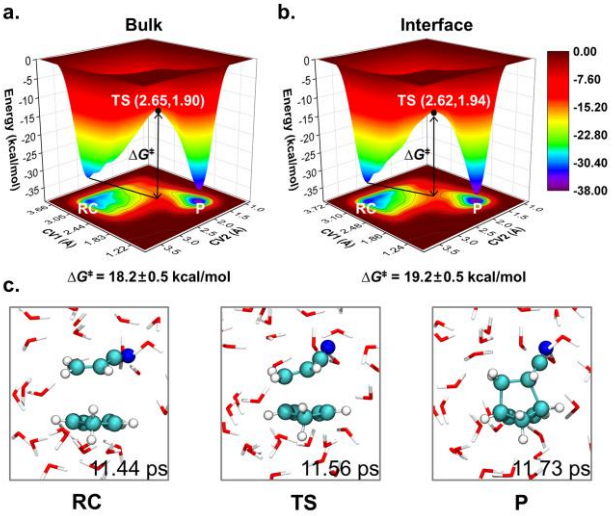

Figure 2. Free-energy landscape of the DA reaction between cyclopentadiene and acrylonitrile (a) in bulk water and (b) at the air-water interface as computed from AIMD+MetD simulations. (c) Snapshots of the RC, TS, and P structures in the simulation of the bulk system. Method: BLYP-D3/DZVP-MOLOPT-SR-GTH.

We attribute the free-energy barrier difference between the air-water interface case and the bulk one to the different stabilization modalities of the RC and TSs. To prove this hypothesis, we have analysed the structures and computed the average number of hydrogen bonds (HBs), n_{HB}, between the N-atom in ALT and the H-atom in water molecules surrounding RC and TS.[70, 72] In the bulk solution, n_{HB} equals to 1.67 and 2.10 for RC and TS, respectively. At the air-water interface, instead, the respective values decrease to 1.48 and 1.82. In comparison, as the system transits from the bulk to the interface, the number of HBs surrounding the TS decreases more than that for the RC, indicating that the TS is destabilized more than the RC as a result of solvent molecule loss. This differential destabilization effect leads to a higher free-energy barrier at the interface. This observation aligns with previous findings.[70, 73-74]

In a nutshell, our simulations indicate the barrier of DA reaction with a partially solvated state at the interface increases with respect to the bulk, so the partial solvation effect cannot be the source for the acceleration of the DA reaction in water microdroplets.

It is known that electric fields (EFs) can affect the reaction kinetics.[60, 75-82] Notably, unlike the EFs at charged tips/electrodes which are directional, the interfacial electric field (IEF) at the surface of a water microdroplet continuously fluctuates over time. Hence, we first computed the barrier change under static and homogeneous external electric fields (EEF) to gain an upper limit of the catalytic effect on the DA reaction, then we examined the effect of the spontaneously fluctuating IEFs at the air-water interface.

Effect of external electric field (EEF). To quantify the impact of EEFs on the DA reaction, we conducted a series of quantum-mechanical calculations where we first applied a uniform static and homogeneous EEF, F, to both the RC and TS along the X, Y, and Z directions, as defined in Figure 1. F_z is aligned along the reaction axis, corresponding to the direction along which the new C–C bonds are forming, whereas F_X/F_Y are aligned perpendicularly to the reaction axis. Molecular structures were optimized under the action of the applied EEF and the resulting energetics are listed in Table 1. It is observed that only applying a positive F_Z lowers the energy barrier, whereas the application of F_X and F_Y raises the height of the barrier. This is consistent with the "reaction-axis rule" proposed by Shaik,[79, 83-84] which states that the application of an EEF along the reaction axis (F_Z here) lowers the barrier, whilst F_X/F_Y induce selectivity between endo- and exo-cycloadducts. Since we are interested in ascertaining the catalytic role of the EEF, we will focus on the results emerging from the application of F_Z only.

Table 1. Calculated potential energy barriers of the DA reaction between CPD and ALT in aqueous (implicit solvation model) and gas phase under static external electric fields (EEFs) of various strengths. Method: M06-2X/6-311++G(d,p).

	$\Delta G^{\ddagger}$ (kcal/mol)					
	Aqueous			Gas		
EEF(V/Å)	F_x	F_y	F_z	F_x	F_y	F_z
0.1	21.7	23.6	17.8	21.8	23.8	20.0
0.05	21.1	20.8	18.5	21.2	21.1	20.1
0	20.0	20.0	20.0	20.8	20.8	20.8
-0.05	20.4	20.0	20.7	20.5	20.9	21.3
-0.1	20.9	20.3	21.8	20.9	21.2	22.0

Figure 3a shows that applying F_z in the positive direction lowers the barrier, whereas in the negative direction it raises the barrier, evidencing that EEFs on the z-axis have either significant catalytic or inhibitory effects on the DA reaction in both gas and aqueous phases.[83] Tracking the energy change of the stationary points (Figure S14) indicates that a positive F_z stabilizes the TS more than the RC, and this different stabilization leads to the barrier decrease. The different response of TS and RC to the EEF aligns with the fact that the Z-component of the dipole moment, μ_Z, is larger for the TS (2.26 D in gas, 3.03 D in aqueous phase) than for the RC (-0.36 D in gas, -0.54 D in aqueous phase). It is known that in the presence of a uniform EEF F_Z, the change in free energy G of a molecular system is approximately $\Delta G = -\mu_{Z,0}F_Z$.[85] Hence, the barrier change subjected to the EEF is $\Delta\Delta G^{\ddagger} = \Delta\mu_{Z,0}^{\ddagger}F_Z$. As shown in Figure 3a, the barrier decrease in presence of F_Z is faster in the aqueous than in the gas phase. This can be explained by the different $\Delta\mu_{Z,0}$ values: 2.62 D in the gas phase and 3.57 D in the liquid.

Inspection of the TS indicates that applying a positive F_Z polarizes the TS structure and hence enhances its asynchronicity. In the aqueous phase, as F_z increases from 0 to 0.1 V/Å, μ_Z of the TS increases from 3.03 D to 4.02 D, because a larger electron density fraction is transferred from the CPD-moiety to the ALT-moiety, where the Mulliken charge of the latter changes from -0.25 e to -0.29 e (Figure S15). At the same time, the C1-C4 bond distance (denoted as CV1) increases and the C2-C3 bond distance (denoted as CV2) decreases. Their difference, $\Delta CV = CV1\text{-}CV2$, is defined as the asynchronicity of the TS. As a result, ΔCV increases from 0.30 Å under field-free

https://doi.org/10.26434/chemrxiv-2024-wwgs1 **ORCID:** https://orcid.org/0000-0001-9676-5734 Content not peer-reviewed by ChemRxiv. **License:** CC BY 4.0

condition to 0.33 Å under F_z = 0.1 V/Å. These observations are in line with the work of Bickelhaupt and Shaik groups.[83, 86]

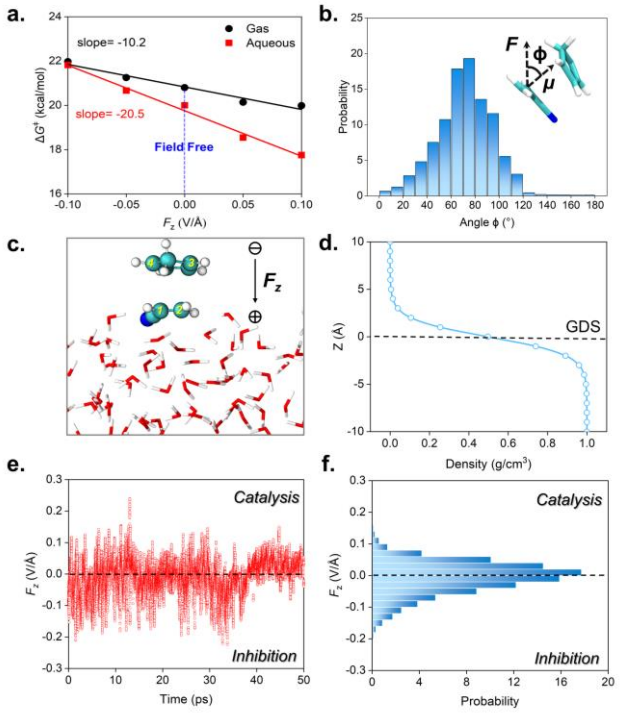

Figure 3. (a) Change of $\Delta G^{\ddagger}$ of DA reaction between CPD and ALT as a function of uniform external electric field F_z in gas (black dots) and aqueous (red squares) phase. (b) Distribution of the angle (ϕ) between the electric field and reactants dipole moment during a simulated trajectory under an external electric field of 0.1 V/Å applied along the z-axis from AIMD+MetD simulations. (c) Model for calculating the electric field generated by interfacial water molecules. (d) Water density profiles from the unbiased AIMD simulation, with the black line marking the Gibbs dividing surface (GDS). (e) Electric field generated by the interfacial water molecules along the z-axis as a function of time from the unbiased AIMD simulation. (f) Statistical distribution of the electric field generated by interfacial water molecules.

When F_Z=0.1 V/Å, the above calculation leads to a barrier drop of 2.2 kcal/mol compared to the field-free condition in the aqueous phase modeled with implicit solvation. To account for the solute-solvent interaction, we further performed AIMD simulations in combination with well-tempered MetD with explicit solvent molecules under a 0.1 V/Å static EEF. Simulation details are present in the Supporting Information. After the application of the EEF, there is a noticeable change in the overall orientation of the water molecules. This can be clearly observed from the snapshots reported in Figure S10 where, compared to the field-free condition, the orientation of water molecules becomes more ordered under the field action. During the simulation, the angle between the EEF and the reactants dipole moment is maintained in a range between 20° and 80° (Figure 3b), an arrangement facilitating the charge transfer from CPD to ALT.

The simulated free-energy barrier changes from 18.2 kcal/mol under field-free condition to 15.8 kcal/mol under a 0.1 V/Å field, leading to a drop of 2.4 kcal/mol (Figure S3), close to the value (2.2 kcal/mol) predicted using an implicit solvent model. This corresponds to roughly 50 times increase in the rate constant using Eyring-Polanyi equation. Committor analysis confirms that the asynchronicity of the TS with explicit solvent molecules also increases under the EEF (Figure S11), where ΔCV increases from 0.75 Å in the zero-field condition to 0.89 Å under F_z = 0.1 V/Å.

Effect of intrinsic interfacial electric field (IEF). Simulations presented above give an upper limit of free-energy barrier change when a possible EF of water microdroplet is perfectly aligned along the reaction coordinate of a given chemical reaction. However, microdroplets interfaces are strongly dynamic entities, making rapidly fluctuating the orientation and magnitude of the IEF, thus affecting its putative catalytic properties. To shed light on this aspect of pivotal concern, we performed unbiased AIMD simulations (i.e., no MetD) to evaluate the genuine distribution of the IEF at the air-water interface by computing the IEF generated by interfacial water molecules along the z-axis of the DA reaction. To do so, we constructed an air-water interface model with 200 water molecules and placed the RC at the interface (Figure S1). The system was simulated for 50 ps, during which the RC was kept fixed while the water molecules were allowed to evolve dynamically by first principles at finite temperature.

Figure 3c shows a snapshot of the AIMD simulation of the RC at the air-water interface and Figure 3d shows the water density profile. The electrostatic potential generated by the Mulliken charges of the water molecules within the interfacial region on RC has been calculated. Specifically, we consider the solvent EF, *F*, calculated at the C1 atom position of RC and oriented along the Z-axis (i.e., reaction axis). The direction of such a Cartesian component is defined in the same way as in Figure 2a, so that a positive value promotes the DA reaction. Computing details are provided in the Supporting Information. Figure 3e depicts that the IEF generated by interfacial water molecules along the reaction axis fluctuates between -0.2 and 0.2 V/Å, with the majority falling within the range of -0.1 to 0.1 V/Å. It is noteworthy that also additional simulations without fixing the RC were performed, leading to similar results (Figure S12). The dynamic nature of the air-water interface and the fluctuating character of the IEF was previously reported also by M. F. Ruiz-López group where they used an OH radical as a probe,[87] as well as T. Head-Gordon group where the IEF was projected onto the O-H bond of a water molecule.[31] According to the 50-ps-long AIMD simulation we report in this work, the resulting time average of the IEF is -0.007 ± 0.0002 V/Å. If we plug this value into the formula $\Delta\Delta G^{\ddagger} = -\Delta\mu_{Z,0}^{\ddagger} F_Z$, and let the value of $\Delta\mu_{Z,0}$ to be 3.1 D, which is the average of the DFT value calculated above in the gas phase (2.62 D) and in aqueous phase (3.57 D, implicit solvent model), it leads to a barrier increase of only ~ 0.02 kcal/mol. Based on this small average value, one might be tempted to conclude that the electrostatic solvation effects on chemical reactivity are negligible. This is inaccurate, because the average value masks the potential role of fluctuations and dynamical effects. Local IEF do have chances to catalyze the reaction when properly oriented along the reaction axis, as represented in the upper half of Figure 3e, f. Nevertheless, the catalytic capability of the IEF might not be as effective as applied spatially and temporarily uniform EEFs since IEFs continuously change both in magnitude and direction as time evolves.

Taken together, aforementioned simulations indicate that 1) partial solvation at air-water interface increases the barrier of the DA reaction (Scheme 1) by about 1 kcal/mol relative to the

https://doi.org/10.26434/chemrxiv-2024-wwgs1 **ORCID:** https://orcid.org/0000-0001-9676-5734 Content not peer-reviewed by ChemRxiv. **License:** CC BY 4.0

bulk; 2) an applied static and homogeneous EEF of 0.1 V/Å is capable of lowering its barrier by about 2 kcal/mol only if oriented along the reaction axis; 3) the air-water IEF fluctuates continuously, rendering its catalytic capability limited as compared to the constant and uniform EEF case. So, the cumulative effect of the partial solvation and IEF may not promote the DA reaction between cyclopentadiene and acrylonitrile in water microdroplets. If, however, this DA reaction was to be accelerated in water microdroplets, other factors should be responsible. To test our computational predictions, a series of experimental investigations were conducted, which are reported in the following section, demonstrating that IEF and partial solvation are not important factors to drive this reaction in microdroplets. Instead, confinement effect becomes predominant.

Mass spectrometry experiment. In the bulk phase, the above DA reaction is known to occur in the presence of a heterogeneous catalyst at an elevated temperature.[88] Cyclopentadiene is highly reactive and undergoes a self-DA reaction, forming dicyclopentadiene. Therefore, we used dicyclopentadiene in our microdroplet experiment, which spontaneously undergoes a retro-DA reaction within the droplet to produce cyclopentadiene (vide infra).[89] We separately prepared two solutions by mixing dicyclopentadiene and acrylonitrile, each with 200 μM concentration, in water and acetonitrile for comparison, followed by atomizing those solutions immediately using a home-built sonic spray source in front of a mass spectrometer inlet (Figure 4a). Unless otherwise stated, the spray source was operated without applying any voltage under a 120-psi nebulizing gas (nitrogen) pressure at a distance of 15 mm from the MS inlet capillary, following a 10 μL/min and 50 μL/min flow rates of water and acetonitrile solutions, respectively, to ensure the recording of ion signals from species at sufficient intensities.

Figure 4b schematically presents the MS detection of different intermediates and products from dicyclopentadiene (**R1**) and acrylonitrile (**R3**) reactions in water or acetonitrile microdroplets (Table S6). In water microdroplets, the dominant reaction was oxidation, forming the ketone **Ox1** from **R1** and ketone **Ox2** from **R2,** as recorded in the corresponding mass spectrum (Figure 4c). These ketones were also characterized by tandem mass spectrometry (Figure S18). However, only a minor extent of the DA reaction, relative to oxidation, was observed in the water microdroplets, as evidenced by detecting a trace level of the product **DA1**. Assuming similar ionization efficiencies for the nitrile compounds (**R3** and **DA1**), the intensity values of these species in the mass spectral data (Figure 4c) indicate that the yield of the DA reaction in water microdroplets is approximately 0.02%. However, the acetonitrile microdroplets were more effective in facilitating the DA reaction, yielding two products (**DA1** and **DA2**) with a combined yield of approximately 0.7% (Figure 4d). Given that the average droplet lifetime is around a few hundred microseconds (see Section III in supporting information), these yields, albeit lower in quantity, suggest a more than 10^6-fold increase of the DA reaction rate in both water and acetonitrile microdroplets compared to the corresponding bulk phase, where the reported rate constant is in the order of 10^{-5} $M^{-1}s^{-1}$.[55] (see Section III in Supporting Information).

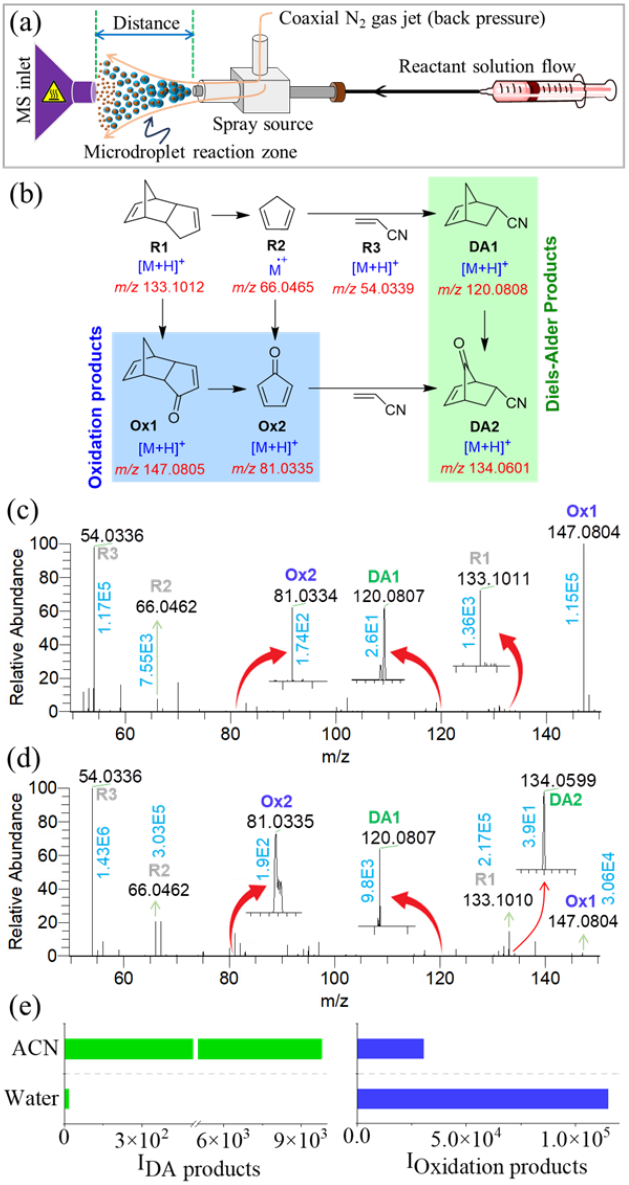

Figure 4. (a) Diagram of the experimental setup for mass spectrometric monitoring of the reaction of dicyclopentadiene and acrylonitrile in microdroplets obtained from a sonic spray source. (b) Schematic presentation of the dual pathways leading to DA and oxidation products in microdroplets as evaluated by MS. The theoretical m/z values of the charged species are indicated below the corresponding structures. The sonic spray (under 0V) mass spectra obtained from spraying a mixture of dicyclopentadiene and acrylonitrile in (c) water and (d) acetonitrile (ACN). The cyan numerical values denote the absolute intensity of the corresponding peak. (e) Histograms showing the screening of the two spray solvents to track the sum of the ion intensities for the DA products (left panel) and oxidation products (right panel), as recorded in the respective mass spectra.

https://doi.org/10.26434/chemrxiv-2024-wwgs1 **ORCID:** https://orcid.org/0000-0001-9676-5734 Content not peer-reviewed by ChemRxiv. **License:** CC BY 4.0

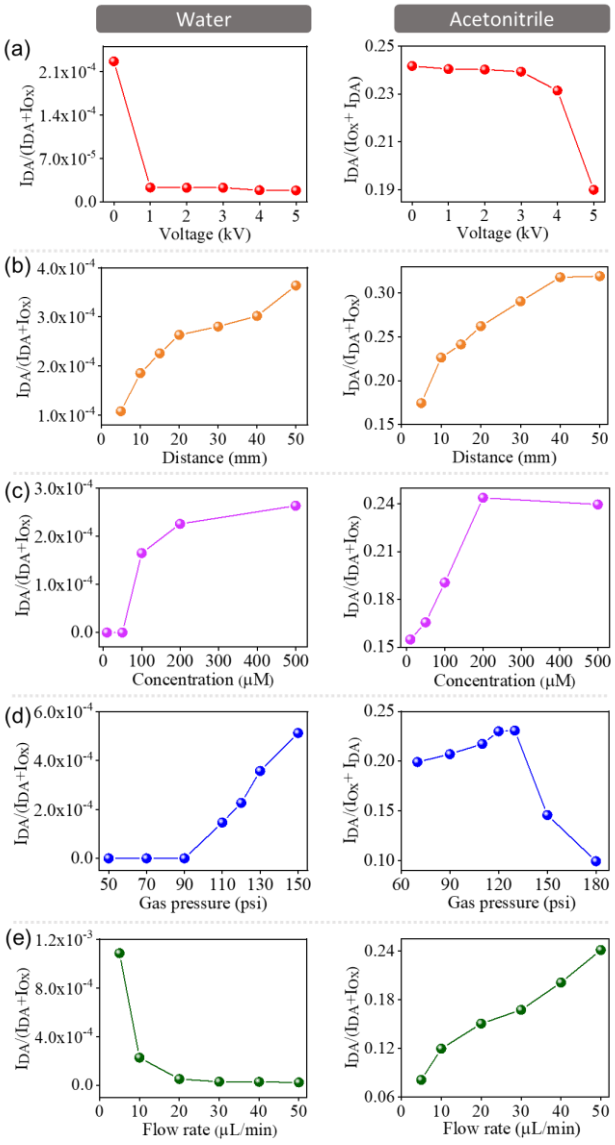

Figure 5. Evaluating the fractional abundance of Diels-Alder (DA) products across all DA and oxidation products in water (left column) and acetonitrile (right column) microdroplets on tuning various spray parameters: (a) spray voltage, (b) distance between spray tip to MS inlet (c) reactant concentration, (d) nebulizing gas pressure, and (e) solution flow rate. The fractional abundance of DA products was calculated using the formula $I_{DA}/(I_{DA}+I_{Ox})$, where I_{DA} represents the sum of the intensities of the DA products, and I_{Ox} denotes the sum of the intensities of the oxidation products.

Although oxidation reactions predominated over DA reactions in both water and acetonitrile droplets (Figures 4c-d), oxidation efficiency was significantly lower in acetonitrile droplets compared to water droplets. This result suggests that microdroplet-generated hydroxyl radicals or reactive oxygen species may play a key role in driving the oxidation of alkane (**R1** and **R2**) to ketone.[10, 12-13, 16, 18, 46, 90] A trace amount of water as an impurity in acetonitrile, or the exposure of the acetonitrile droplets to moisture in the air might have driven the observed oxidation reaction (Figure 4d). Figure 4e presents the histogram compiling the above results, showing that oxidation occurred effectively in water droplets, while the DA reaction was relatively more prominent in acetonitrile droplets. To explore the reasons behind these differences and identify factors that might influence the DA reactions in microdroplets, we assessed the reactions under various spray conditions.

We measured the fractional abundance of DA products across all products (**Ox1**, **Ox2**, **DA1**, and **DA2**) in the mass spectra recorded by tuning the spray parameters. When a spray potential was applied to generate a charged microdroplet surface, which subsequently increases the interfacial electric field,[35] the extent of the DA reaction in water droplets decreased significantly compared to acetonitrile droplets (Figure 5a). This result indicates a marked preference for oxidation reactions at the charged surface of water microdroplets at the expense of the competing DA reactions (Figure S19), which may not prefer the charged environment of the droplet and, hence, the associated electric field at the surface. In other words, the IEF has a negligible role in promoting the DA reactions, as predicted by our simulations using both water and acetonitrile as solvent (Table S4). Instead, the IEF triggers oxidation reactions.

As increasing the distance between the spray source and the MS inlet increases the microdroplet reaction time and reduces the droplet size by its evolution (evaporation/fission) process, we tuned this distance to monitor its effect on the microdroplet reaction. Surprisingly, the increased flight time and subsequent evaporation of the microdroplets led to a higher fractional abundance of DA products (Figure 5b). This result suggests that the trace level of the DA reaction observed in water microdroplets is possibly caused by the confinement or increased concentration of reactants in a small volume during the microdroplet evolution. Indeed, when we gradually increased the reactant concentration in microdroplets, the efficacy of the DA reaction improved (Figure 5c). The increased nebulizing gas pressure in the spray source is known to cause faster droplet solvent evaporation and fission, producing smaller droplets with a high surface-to-volume ratio.[91-92] When we raised the gas pressure, the tendency of the DA reaction in water microdroplets continued to increase (Figure 5d). This suggests that the DA reaction might predominantly occur at the air-water interface, facilitated by the accumulation (increased concentration) of hydrophobic reactants at that location. The acetonitrile droplet also exhibited a similar reaction trend up to a certain gas pressure (130 psi), after which the propensity of DA reaction decreased (Figure 5d). This result might be explained by the possible distribution of hydrophobic reactants throughout the acetonitrile droplet, allowing the DA reaction to occur both at the interface and within the core of the acetonitrile droplet, which is in contrast to the water droplet case as discussed above.

However, the oxidation reaction in either acetonitrile or water droplets is expected to occur primarily at the droplet surface, where reactive oxygen species are more prevalent. The rapid evaporation of acetonitrile results in a substantial increase in the surface-to-volume ratio of acetonitrile microdroplets at elevated nebulizing gas pressures (>130 psi), promoting oxidation reactions at the expense of DA reactions at the interface. This hypothesis is supported by studies investigating the impact of varying spray solution flow rates on the reactions (Figure 5e). Ramping up the flow rate of the spray solution leads to larger microdroplets with a decreased surface-to-volume ratio. As both DA and oxidation reactions are expected to occur at the surface of water microdroplets, the efficacy of both these reactions decreased with the increase in the aqueous solution flow rate. However, the DA reaction experienced a more pronounced

https://doi.org/10.26434/chemrxiv-2024-wwgs1 **ORCID:** https://orcid.org/0000-0001-9676-5734 Content not peer-reviewed by ChemRxiv. **License:** CC BY 4.0

decrease than the oxidation reaction, reducing the fractional abundance of DA products with an increasing flow rate (Figure 5e). This result again points to the effect of polar water on enhancing the local concentration of hydrophobic reagents at the air-water interface to impart the DA reaction, albeit with a lower propensity compared to the dominant oxidation reactions. In contrast, the impact of the acetonitrile flow rate on the DA reaction was different, i.e., the fractional abundance of DA products increased by increasing the flow rate (Figure 5d). This result indicates that the DA reaction in acetonitrile microdroplets is not restricted solely to its surface but predominantly extends throughout its core. The increased solution mass flow supplied a greater quantity of reagents per droplet, and due to the rapid evaporation of acetonitrile, the droplet became enriched with reagents confined in a small space, which subsequently impacted the DA reaction inside the acetonitrile droplet.

CONCLUSIONS

By the means of a series of simulation approaches and experimental investigations, we explore the acceleration phenomenon (i.e., catalysis) of a Diels-Alder (DA) reaction between cyclopentadiene and acrylonitrile in water microdroplets. Quantum-mechanical calculations and first-principles molecular dynamics coupled with enhanced sampling techniques revealed that the partial solvation effect and local interfacial electric field at the water microdroplet surface are not factors accelerating the DA reaction. Specifically, the free-energy barrier of the DA reaction at the water microdroplet interface was found to be approximately 1 kcal/mol higher compared to the bulk phase one. Although the presence of a local strong electric field at the gas-liquid interface could slightly decrease the barrier by about 2 kcal/mol along the reaction axis, the fluctuating nature of this interfacial electric field significantly inhibits its catalytic effect on the DA reaction. These predictions were confirmed by microdroplet experiments.

Experimentally, the DA reaction is not as highly favored as oxidation reactions in water microdroplets. However, the detection of trace levels (0.02%) of DA products from the reaction between dicyclopentadiene and acrylonitrile in water microdroplets is attributed to the surface enrichment of these hydrophobic reactants on the droplet surface. The increased polarity (or charge) or electric field on such droplet surfaces inhibits the DA reaction by promoting substrate oxidation, indicating that the local electric field does not facilitate the DA reaction at the air-water interface. Additionally, the study, dependent on spray parameters, revealed that while the DA reaction might occur at the surface of water microdroplets, it prefers to occur within the core of acetonitrile droplets, suggesting that partial solvation is not necessarily a critical factor for this reaction. Instead, the confinement effect caused by rapid evaporation is the driving force for acceleration of the DA reaction in microdroplets. This work provides insights for manipulating reactions in water microdroplets, offering potential perspectives on leveraging water microdroplet chemistry for future applications.

ASSOCIATED CONTENT

Supporting Information.
Experimental and theoretical methods, supplementary experimental and theoretical results, and computational raw data. This material is available free of charge via the Internet at http://pubs.acs.org.

Notes
The authors declare no competing financial interests.

ACKNOWLEDGMENT

J.X. acknowledges financial support from the National Natural Science Foundation of China (no. 22273004), Beijing Natural Science Foundation (no. 2222028), and the Teli Fellowship from Beijing Institute of Technology, China. S.B. acknowledged support from Science and Engineering Research Board, India (grant number CRG/2022/002676). G.C. acknowledges financial support from ICSC – Centro Nazionale di Ricerca in High-Performance Computing, Big Data and Quantum Computing, funded by European Union – NextGenerationEU - PNRR, Missione 4 Componente 2 Investimento 1.4. G.C. acknowledges the European Union – NextGeneration EU from the Italian Ministry of Environment and Energy Security POR H2 AdP MMES/ENEA with involvement of CNR and RSE, PNRR - Mission 2, Component 2, Investment 3.5 "Ricerca e sviluppo sull'idrogeno", CUP: B93C22000630006. G.C. acknowledges the European Union (NextGeneration EU), through the MUR-PNRR project SAMOTHRACE (ECS00000022). G.C. is thankful to CINECA for awards under the ISCRA initiative for the availability of high-performance computing resources and support. A. H. also acknowledges funding by the European Union (ERC, HyBOP, Grant Number: 101043272). Views and opinions expressed are however those of the author(s) only and do not necessarily reflect those of the European Union or the European Research Council. Neither the European Union nor the granting authority can be held responsible for them. The authors thank Prof. Michelle L. Coote for helpful discussions.

Author Contributions
[#]K.G. and N. A. contributed equally to this work.

Notes
The authors declare no competing financial interests.

REFERENCES

(1) Banerjee, S.; Zare, R. N., Syntheses of Isoquinoline and Substituted Quinolines in Charged Microdroplets. *Angew. Chem. Int. Ed.* **2015,** *54* (49), 14795-14799.
(2) Girod, M.; Moyano, E.; Campbell, D. I.; Cooks, R. G., Accelerated bimolecular reactions in microdroplets studied by desorption electrospray ionization mass spectrometry. *Chem. Sci.* **2011,** *2* (3), 501-510.
(3) Lai, Y.-H.; Sathyamoorthi, S.; Bain, R. M.; Zare, R. N., Microdroplets Accelerate Ring Opening of Epoxides. *J. Am. Soc. Mass Spectrom.* **2018,** *29* (5), 1036-1043.
(4) Lee, J. K.; Banerjee, S.; Nam, H. G.; Zare, R. N., Acceleration of reaction in charged microdroplets. *Q. Rev. Biophys.* **2015,** *48* (4), 437-444.
(5) Song, Z.; Liang, C.; Gong, K.; Zhao, S.; Yuan, X.; Zhang, X.; Xie, J., Harnessing the High Interfacial Electric Fields on Water Microdroplets to Accelerate Menshutkin Reactions. *J. Am. Chem. Soc.* **2023,** *145* (48), 26003-26008.
(6) Chen, H.; Wang, R.; Xu, J.; Yuan, X.; Zhang, D.; Zhu, Z.; Marshall, M.; Bowen, K.; Zhang, X., Spontaneous Reduction by One Electron on Water Microdroplets Facilitates Direct Carboxylation with CO_2. *J. Am. Chem. Soc.* **2023,** *145* (4), 2647-2652.
(7) Eremin, D. B.; Fokin, V. V., On-Water Selectivity Switch in Microdroplets in the 1,2,3-Triazole Synthesis from Bromoethenesulfonyl Fluoride. *J. Am. Chem. Soc.* **2021,** *143* (44), 18374-18379.

https://doi.org/10.26434/chemrxiv-2024-wwgs1 **ORCID:** https://orcid.org/0000-0001-9676-5734 Content not peer-reviewed by ChemRxiv. **License:** CC BY 4.0

(8) Gnanamani, E.; Yan, X.; Zare, R. N., Chemoselective N-Alkylation of Indoles in Aqueous Microdroplets. *Angew. Chem. Int. Ed.* **2020,** *59* (8), 3069-3072.
(9) Holden, D. T.; Morato, N. M.; Cooks, R. G., Aqueous microdroplets enable abiotic synthesis and chain extension of unique peptide isomers from free amino acids. *Proc. Natl. Acad. Sci.* **2022,** *119* (42), e2212642119.
(10) Meng, Y.; Gnanamani, E.; Zare, R. N., Direct C(sp^3)–N Bond Formation between Toluene and Amine in Water Microdroplets. *J. Am. Chem. Soc.* **2022,** *144* (43), 19709-19713.
(11) Meng, Y.; Gnanamani, E.; Zare, R. N., One-Step Formation of Pharmaceuticals Having a Phenylacetic Acid Core Using Water Microdroplets. *J. Am. Chem. Soc.* **2023,** *145* (14), 7724-7728.
(12) Meng, Y.; Gnanamani, E.; Zare, R. N., Catalyst-Free Decarboxylative Amination of Carboxylic Acids in Water Microdroplets. *J. Am. Chem. Soc.* **2023,** *145* (1), 32-36.
(13) Meng, Y.; Zare, R. N.; Gnanamani, E., One-Step, Catalyst-Free Formation of Phenol from Benzoic Acid Using Water Microdroplets. *J. Am. Chem. Soc.* **2023,** *145* (35), 19202-19206.
(14) Nam, I.; Lee, J. K.; Nam, H. G.; Zare, R. N., Abiotic production of sugar phosphates and uridine ribonucleoside in aqueous microdroplets. *Proc. Natl. Acad. Sci.* **2017,** *114* (47), 12396-12400.
(15) Nandy, A.; Kumar, A.; Mondal, S.; Koner, D.; Banerjee, S., Spontaneous Generation of Aryl Carbocations from Phenols in Aqueous Microdroplets: Aromatic SN1 Reactions at the Air–Water Interface. *J. Am. Chem. Soc.* **2023,** *145* (29), 15674-15679.
(16) Song, X.; Basheer, C.; Xia, Y.; Li, J.; Abdulazeez, I.; Al-Saadi, A. A.; Mofidfar, M.; Suliman, M. A.; Zare, R. N., One-step Formation of Urea from Carbon Dioxide and Nitrogen Using Water Microdroplets. *J. Am. Chem. Soc.* **2023,** *145* (47), 25910-25916.
(17) Song, X.; Basheer, C.; Zare, R. N., Making ammonia from nitrogen and water microdroplets. *Proc. Natl. Acad. Sci.* **2023,** *120* (16), e2301206120.
(18) Song, X.; Meng, Y.; Zare, R. N., Spraying Water Microdroplets Containing 1,2,3-Triazole Converts Carbon Dioxide into Formic Acid. *J. Am. Chem. Soc.* **2022,** *144* (37), 16744-16748.
(19) Wang, T.; Li, Z.; Gao, H.; Hu, J.; Chen, H.-Y.; Xu, J.-J., Ultrafast C–C and C–N bond formation reactions in water microdroplets facilitated by the spontaneous generation of carbocations. *Chem. Sci.* **2023,** *14* (41), 11515-11520.
(20) Zhang, D.; Yuan, X.; Gong, C.; Zhang, X., High Electric Field on Water Microdroplets Catalyzes Spontaneous and Ultrafast Oxidative C–H/N–H Cross-Coupling. *J. Am. Chem. Soc.* **2022,** *144* (35), 16184-16190.
(21) Zhao, L.; Song, X.; Gong, C.; Zhang, D.; Wang, R.; Zare, R. N.; Zhang, X., Sprayed water microdroplets containing dissolved pyridine spontaneously generate pyridyl anions. *Proc. Natl. Acad. Sci.* **2022,** *119* (12), e2200991119.
(22) Zhu, C.; Pham, L. N.; Yuan, X.; Ouyang, H.; Coote, M. L.; Zhang, X., High Electric Fields on Water Microdroplets Catalyze Spontaneous and Fast Reactions in Halogen-Bond Complexes. *J. Am. Chem. Soc.* **2023,** *145* (39), 21207-21212.
(23) Nandy, A.; Mondal, S.; Koner, D.; Banerjee, S., Heavy Water Microdroplet Surface Enriches the Lighter Isotopologue Impurities. *J. Am. Chem. Soc.* **2024**.
(24) Chen, X.; Xia, Y.; Zhang, Z.; Hua, L.; Jia, X.; Wang, F.; Zare, R. N., Hydrocarbon Degradation by Contact with Anoxic Water Microdroplets. *J. Am. Chem. Soc.* **2023,** *145* (39), 21538-21545.
(25) Gong, K.; Meng, Y.; Zare, R. N.; Xie, J., Molecular Mechanism for Converting Carbon Dioxide Surrounding Water Microdroplets Containing 1,2,3-Triazole to Formic Acid. *J. Am. Chem. Soc.* **2024,** *146* (12), 8576-8584.
(26) Jin, S.; Chen, H.; Yuan, X.; Xing, D.; Wang, R.; Zhao, L.; Zhang, D.; Gong, C.; Zhu, C.; Gao, X.; Chen, Y.; Zhang, X., The Spontaneous Electron-Mediated Redox Processes on Sprayed Water Microdroplets. *JACS Au* **2023,** *3* (6), 1563-1571.
(27) Kumar, A.; Mondal, S.; Banerjee, S., Aqueous Microdroplets Capture Elusive Carbocations. *J. Am. Chem. Soc.* **2021,** *143* (6), 2459-2463.
(28) Kumar, A.; Mondal, S.; Mofidfar, M.; Zare, R. N.; Banerjee, S., Capturing Reactive Carbanions by Microdroplets. *J. Am. Chem. Soc.* **2022,** *144* (17), 7573-7577.
(29)Kumar, A.; Mondal, S.; Sandeep; Venugopalan, P.; Kumar, A.; Banerjee, S., Destabilized Carbocations Caged in Water Microdroplets: Isolation and Real-Time Detection of α-Carbonyl Cation Intermediates. *J. Am. Chem. Soc.* **2022,** *144* (8), 3347-3352.
(30) Chamberlayne, C. F.; Zare, R. N., Simple model for the electric field and spatial distribution of ions in a microdroplet. *J. Chem. Phys.* **2020,** *152* (18), 184702.
(31) Xiong, H.; Lee, J. K.; Zare, R. N.; Min, W., Strong electric field observed at the interface of aqueous microdroplets. *J. Phys. Chem. Lett.* **2020,** *11* (17), 7423-7428.
(32) Hao, H.; Leven, I.; Head-Gordon, T., Can electric fields drive chemistry for an aqueous microdroplet? *Nat. Commun.* **2022,** *13* (1), 280.
(33) Qiu, L.; Wei, Z.; Nie, H.; Cooks, R. G., Reaction Acceleration Promoted by Partial Solvation at the Gas/Solution Interface. *ChemPlusChem* **2021,** *86* (10), 1362-1365.
(34) Wei, Z.; Li, Y.; Cooks, R. G.; Yan, X., Accelerated Reaction Kinetics in Microdroplets: Overview and Recent Developments. *Annu. Rev. Phys. Chem.* **2020,** *71* (1), 31-51.
(35) Banerjee, S., On the stability of carbocation in water microdroplets. *Int. J. Mass spectrom.* **2023,** *486*, 117024.
(36) Colussi, A. J.; Enami, S.; Ishizuka, S., Hydronium Ion Acidity Above and Below the Interface of Aqueous Microdroplets. *ACS Earth Space Chem.* **2021,** *5* (9), 2341-2346.
(37) Li, K.; Gong, K.; Liu, J.; Ohnoutek, L.; Ao, J.; Liu, Y.; Chen, X.; Xu, G.; Ruan, X.; Cheng, H.; Han, J.; Sui, G.; Ji, M.; Valev, V. K.; Zhang, L., Significantly accelerated photochemical and photocatalytic reactions in microdroplets. *Cell Rep. Phys. Sci.* **2022,** *3* (6), 100917.
(38) Li, M.; Kan, Y.; Su, H.; Pöschl, U.; Parekh, S. H.; Bonn, M.; Cheng, Y., Spatial homogeneity of pH in aerosol microdroplets. *Chem* **2023,** *9* (4), 1036-1046.
(39) Wei, H.; Vejerano, E. P.; Leng, W.; Huang, Q.; Willner, M. R.; Marr, L. C.; Vikesland, P. J., Aerosol microdroplets exhibit a stable pH gradient. *Proc. Natl. Acad. Sci.* **2018,** *115* (28), 7272-7277.
(40) Feng, C.; Zhang, L., Microdroplet assisted hollow ZnCdS@PDA nanocages' synergistic confinement effect for promoting photocatalytic H_2O_2 production. *Mater. Horiz.* **2024,** *11* (6), 1515-1527.
(41)Briones, A. M.; Ervin, J. S.; Byrd, L. W.; Putnam, S. A.; White, A.; Jones, J. G., Evaporation Characteristics of Pinned Water Microdroplets. *J. Thermophys. Heat Transfer* **2012,** *26* (3), 480-493.
(42) Chen, C. J.; Williams, E. R., The role of analyte concentration in accelerated reaction rates in evaporating droplets. *Chem. Sci.* **2023,** *14* (18), 4704-4713.
(43) Marsh, B. M.; Iyer, K.; Cooks, R. G., Reaction Acceleration in Electrospray Droplets: Size, Distance, and Surfactant Effects. *J. Am. Soc. Mass Spectrom.* **2019,** *30* (10), 2022-2030.
(44) Putnam, S. A.; Briones, A. M.; Byrd, L. W.; Ervin, J. S.; Hanchak, M. S.; White, A.; Jones, J. G., Microdroplet evaporation on superheated surfaces. *Int. J. Heat Mass Transfer* **2012,** *55* (21), 5793-5807.
(45) Rovelli, G.; Jacobs, M. I.; Willis, M. D.; Rapf, R. J.; Prophet, A. M.; Wilson, K. R., A critical analysis of electrospray techniques for the determination of accelerated rates and mechanisms of chemical reactions in droplets. *Chem. Sci.* **2020,** *11* (48), 13026-13043.
(46) Gallo Jr, A.; Musskopf, N. H.; Liu, X.; Yang, Z.; Petry, J.; Zhang, P.; Thoroddsen, S.; Im, H.; Mishra, H., On the formation of

https://doi.org/10.26434/chemrxiv-2024-wwgs1 **ORCID:** https://orcid.org/0000-0001-9676-5734 Content not peer-reviewed by ChemRxiv. **License:** CC BY 4.0

hydrogen peroxide in water microdroplets. *Chem. Sci.* **2022,** *13* (9), 2574-2583.
(47) Mofidfar, M.; Mehrgardi, M. A.; Xia, Y.; Zare, R. N., Dependence on relative humidity in the formation of reactive oxygen species in water droplets. *Proc. Natl. Acad. Sci.* **2024,** *121* (12), e2315940121.
(48) Wang, S.; Yang, J.; Liu, F.; Xiao, S.; Xiao, F.; Dong, X.; Shan, S., Water microdroplets: A catalyst-free source of reactive oxygen species for pollutants removal. *J. Cleaner Prod.* **2023,** *420*, 138444.
(49)Corey, E. J., Catalytic Enantioselective Diels–Alder Reactions: Methods, Mechanistic Fundamentals, Pathways, and Applications. *Angew. Chem. Int. Ed.* **2002,** *41* (10), 1650-1667.
(50) Pindur, U.; Lutz, G.; Otto, C., Acceleration and selectivity enhancement of Diels-Alder reactions by special and catalytic methods. *Chem. Rev.* **1993,** *93* (2), 741-761.
(51) Schlueter, J. A.; Seaman, J. M.; Taha, S.; Cohen, H.; Lykke, K. R.; Wang, H. H.; Williams, J. M., Synthesis, purification, and characterization of the 1 : 1 addition product of C60 and anthracene. *J. Chem. Soc., Chem. Commun.* **1993**, 972-974.
(52) Tsuda, M.; Ishida, T.; Nogami, T.; Kurono, S.; Ohashi, M., Isolation and characterization of Diels–Alder adducts of C60 with anthracene and cyclopentadiene. *J. Chem. Soc., Chem. Commun.* **1993**, 1296-1298.
(53) Breslow, R.; Maitra, U., On the origin of product selectivity in aqueous diels-alder reactions. *Tetrahedron Lett.* **1984,** *25* (12), 1239-1240.
(54) Breslow, R.; Maitra, U.; Rideout, D., Selective diels-alder reactions in aqueous solutions and suspensions. *Tetrahedron Lett.* **1983,** *24* (18), 1901-1904.
(55) Rideout, D. C.; Breslow, R., Hydrophobic acceleration of Diels-Alder reactions. *J. Am. Chem. Soc.* **1980,** *102* (26), 7816-7817.
(56) Narayan, S.; Muldoon, J.; Finn, M. G.; Fokin, V. V.; Kolb, H. C.; Sharpless, K. B., "On Water": Unique Reactivity of Organic Compounds in Aqueous Suspension. *Angew. Chem. Int. Ed.* **2005,** *44* (21), 3275-3279.
(57) Banerjee, S.; Gnanamani, E.; Yan, X.; Zare, R. N., Can all bulk-phase reactions be accelerated in microdroplets? *Analyst* **2017,** *142* (9), 1399-1402.
(58) Bain, R. M.; Sathyamoorthi, S.; Zare, R. N., "On-Droplet" Chemistry: The Cycloaddition of Diethyl Azodicarboxylate and Quadricyclane. *Angew. Chem. Int. Ed.* **2017,** *56* (47), 15083-15087.
(59) Chen, H.; Wang, R.; Chiba, T.; Foreman, K.; Bowen, K.; Zhang, X., Designer "Quasi-Benzyne": The Spontaneous Reduction of Ortho-Diiodotetrafluorobenzene on Water Microdroplets. *J. Am. Chem. Soc.* **2024,** *146* (15), 10979-10983.
(60) Aragonès, A. C.; Haworth, N. L.; Darwish, N.; Ciampi, S.; Bloomfield, N. J.; Wallace, G. G.; Diez-Perez, I.; Coote, M. L., Electrostatic catalysis of a Diels–Alder reaction. *Nature* **2016,** *531* (7592), 88-91.
(61) Kühne, T. D.; Iannuzzi, M.; Del Ben, M.; Rybkin, V. V.; Seewald, P.; Stein, F.; Laino, T.; Khaliullin, R. Z.; Schütt, O.; Schiffmann, F.; Golze, D.; Wilhelm, J.; Chulkov, S.; Bani-Hashemian, M. H.; Weber, V.; Borštnik, U.; Taillefumier, M.; Jakobovits, A. S.; Lazzaro, A.; Pabst, H.; Müller, T.; Schade, R.; Guidon, M.; Andermatt, S.; Holmberg, N.; Schenter, G. K.; Hehn, A.; Bussy, A.; Belleflamme, F.; Tabacchi, G.; Glöß, A.; Lass, M.; Bethune, I.; Mundy, C. J.; Plessl, C.; Watkins, M.; VandeVondele, J.; Krack, M.; Hutter, J., CP2K: An electronic structure and molecular dynamics software package - Quickstep: Efficient and accurate electronic structure calculations. *J. Chem. Phys.* **2020,** *152* (19), 194103.
(62) Barducci, A.; Bussi, G.; Parrinello, M., Well-Tempered Metadynamics: A Smoothly Converging and Tunable Free-Energy Method. *Phys. Rev. Lett.* **2008,** *100* (2), 020603.
(63) Goedecker, S.; Teter, M.; Hutter, J., Separable dual-space Gaussian pseudopotentials. *Phys. Rev. B* **1996,** *54* (3), 1703.
(64) Hartwigsen, C.; Gœdecker, S.; Hutter, J., Relativistic separable dual-space Gaussian pseudopotentials from H to Rn. *Phys. Rev. B* **1998,** *58* (7), 3641.
(65) VandeVondele, J.; Hutter, J., Gaussian basis sets for accurate calculations on molecular systems in gas and condensed phases. *J. Chem. Phys.* **2007,** *127* (11), 114105.
(66) Becke, A. D., Density-functional exchange-energy approximation with correct asymptotic behavior. *Phys. Rev. A* **1988,** *38* (6), 3098.
(67) Frisch, M.; Trucks, G.; Schlegel, H.; Scuseria, G.; Robb, M.; Cheeseman, J.; Scalmani, G.; Barone, V.; Petersson, G.; Nakatsuji, H., Gaussian 16, Revision A. 03, Gaussian. *Inc., Wallingford CT* **2016,** *3*.
(68) Krishnan, R.; Binkley, J. S.; Seeger, R.; Pople, J. A., Self-consistent molecular orbital methods. XX. A basis set for correlated wave functions. *J. Chem. Phys.* **1980,** *72* (1), 650-654.
(69) Zhao, Y.; Truhlar, D. G., The M06 suite of density functionals for main group thermochemistry, thermochemical kinetics, noncovalent interactions, excited states, and transition elements: two new functionals and systematic testing of four M06-class functionals and 12 other functionals. *Theor. Chem. Acc.* **2008,** *120* (1), 215-241.
(70) Thomas, L. L.; Tirado-Rives, J.; Jorgensen, W. L., Quantum Mechanical/Molecular Mechanical Modeling Finds Diels−Alder Reactions Are Accelerated Less on the Surface of Water Than in Water. *J. Am. Chem. Soc.* **2010,** *132* (9), 3097-3104.
(71) Di Pino, S.; Perez Sirkin, Y. A.; Morzan, U. N.; Sánchez, V. M.; Hassanali, A.; Scherlis, D. A., Water Self-Dissociation is Insensitive to Nanoscale Environments. *Angew. Chem. Int. Ed.* **2023,** *62* (34), e202306526.
(72) Pestana, L. R.; Hao, H.; Head-Gordon, T., Diels–Alder Reactions in Water Are Determined by Microsolvation. *Nano Lett.* **2020,** *20* (1), 606-611.
(73) Chandrasekhar, J.; Shariffskul, S.; Jorgensen, W. L., QM/MM Simulations for Diels−Alder Reactions in Water: Contribution of Enhanced Hydrogen Bonding at the Transition State to the Solvent Effect. *J. Phys. Chem. B* **2002,** *106* (33), 8078-8085.
(74) Soto-Delgado, J.; Tapia, R. A.; Torras, J., Multiscale Treatment for the Molecular Mechanism of a Diels–Alder Reaction in Solution: A QM/MM-MD Study. *J. Chem. Theory Comput.* **2016,** *12* (10), 4735-4742.
(75) Cassone, G., Nuclear Quantum Effects Largely Influence Molecular Dissociation and Proton Transfer in Liquid Water under an Electric Field. *J. Phys. Chem. Lett.* **2020,** *11* (21), 8983-8988.
(76) Cassone, G.; Pietrucci, F.; Saija, F.; Guyot, F.; Saitta, A. M., One-step electric-field driven methane and formaldehyde synthesis from liquid methanol. *Chem. Sci.* **2017,** *8* (3), 2329-2336.
(77) Cassone, G.; Sofia, A.; Rinaldi, G.; Sponer, J., Catalyst-Free Hydrogen Synthesis from Liquid Ethanol: An ab Initio Molecular Dynamics Study. *J. Phys. Chem. C* **2019,** *123* (14), 9202-9208.
(78) Fried, S. D.; Bagchi, S.; Boxer, S. G., Extreme electric fields power catalysis in the active site of ketosteroid isomerase. *Science* **2014,** *346* (6216), 1510-1514.
(79) Shaik, S.; Ramanan, R.; Danovich, D.; Mandal, D., Structure and reactivity/selectivity control by oriented-external electric fields. *Chem. Soc. Rev.* **2018,** *47* (14), 5125-5145.
(80) Welborn, V. V.; Ruiz Pestana, L.; Head-Gordon, T., Computational optimization of electric fields for better catalysis design. *Nat. Catal.* **2018,** *1* (9), 649-655.
(81) Zhang, Y.; Jiang, B., Universal machine learning for the response of atomistic systems to external fields. *Nat. Commun.* **2023,** *14* (1), 6424.
(82) Shaik, S. S.; Stuyver, T., *Effects of electric fields on structure and reactivity: new horizons in chemistry*. Royal Society of Chemistry: 2021.

https://doi.org/10.26434/chemrxiv-2024-wwgs1 **ORCID:** https://orcid.org/0000-0001-9676-5734 Content not peer-reviewed by ChemRxiv. **License:** CC BY 4.0

(83) Meir, R.; Chen, H.; Lai, W.; Shaik, S., Oriented electric fields accelerate Diels–Alder reactions and control the endo/exo selectivity. *ChemPhysChem* **2010,** *11* (1), 301-310.
(84) Ramanan, R.; Danovich, D.; Mandal, D.; Shaik, S., Catalysis of Methyl Transfer Reactions by Oriented External Electric Fields: Are Gold–Thiolate Linkers Innocent? *J. Am. Chem. Soc.* **2018,** *140* (12), 4354-4362.
(85) Hoffmann, N. M.; Wang, X.; Berkelbach, T. C., Linear Free Energy Relationships in Electrostatic Catalysis. *ACS Catal.* **2022,** *12* (14), 8237-8241.
(86) Yu, S.; Vermeeren, P.; Hamlin, T. A.; Bickelhaupt, F. M., How Oriented External Electric Fields Modulate Reactivity. *Chem. Eur. J.* **2021,** *27* (18), 5683-5693.
(87) Martins-Costa, M. T. C.; Ruiz-López, M. F., Electrostatics and Chemical Reactivity at the Air–Water Interface. *J. Am. Chem. Soc.* **2023,** *145* (2), 1400-1406.
(88) Parlar, H.; Baumann, R., Diels-Alder Reaction of Cyclopentadiene with Acrylic Acid Derivatives in Heterogeneous Phases. *Angew. Chem. Int. Ed.* **1981,** *20* (12), 1014-1014.
(89) Dickson, R. S.; Dobney, B. J.; Eastwood, F. W., Preparation of cyclopentadiene from its dimer. *J. Chem. Educ.* **1987,** *64* (10), 898.
(90) Kumar, A.; Avadhani, V. S.; Nandy, A.; Mondal, S.; Pathak, B.; Pavuluri, V. K. N.; Avulapati, M. M.; Banerjee, S., Water Microdroplets in Air: A Hitherto Unnoticed Natural Source of Nitrogen Oxides. *Anal. Chem.* **2024,** *96* (26), 10515-10523.
(91) Banerjee, S.; Mazumdar, S., Electrospray Ionization Mass Spectrometry: A Technique to Access the Information beyond the Molecular Weight of the Analyte. *Int. J. Anal. Chem.* **2012,** *2012* (1), 282574.
(92) Gao, D.; Jin, F.; Lee, J. K.; Zare, R. N., Aqueous microdroplets containing only ketones or aldehydes undergo Dakin and Baeyer–Villiger reactions. *Chem. Sci.* **2019,** *10* (48), 10974-10978.

https://doi.org/10.26434/chemrxiv-2024-wwgs1 **ORCID:** https://orcid.org/0000-0001-9676-5734 Content not peer-reviewed by ChemRxiv. **License:** CC BY 4.0